

Cu₂SnS₃ thin films deposited by spin coating route: a promise candidate for low cost, safe and flexible solar cells

H. Dahman¹ · L. El Mir^{1,2}

Received: 16 March 2015 / Accepted: 8 May 2015 / Published online: 16 May 2015
© Springer Science+Business Media New York 2015

Abstract Thin films of Cu₂SnS₃ (CTS) was successfully grown on glass substrates by sol–gel spin coating technique. In this work, the effect of drying time on structural, morphological and optical characteristics is investigated while drying temperature was kept at 300 °C. The samples were characterized by means of X-ray diffraction (XRD), scanning electron microscopy (SEM), atomic force microscopy (AFM), UV–Vis–NIR spectroscopy and four probe analysis. The XRD patterns of the samples proved the polycrystalline nature and the formation of pure cubic Cu₂SnS₃ structure with (111) preferential orientation. No peak referring to other binary or ternary phases were detected in the patterns. The average crystallite sizes calculated using the Debye–Scherrer formula was about 7.5 nm. The AFM and SEM images revealed that the CTS films have continuous and dense morphology. The films roughness increases from 8 to 68 nm with increasing drying time from 2 to 10 min. The thin films absorption coefficients were in the range 0.66×10^5 – 1.38×10^5 cm⁻¹ at 2.14 eV. We found that by increasing the drying time, the sheet resistance increased from 22 to 574 kΩ and the direct optical band gap increased from 1.19 to 1.65 eV. The synthesised material seems to be a good candidate for flexible, cheap and friendly environment solar cells applications.

1 Introduction

The limitation of conventional sources with fossil fuels and the constantly increasing of global need of energy give great importance to the conversion of energy by the photovoltaic technology which should reach the terawatt scale.

Despite their outdoor stability, great technical promise of CuInGa(S,Se)₂ (CIGS) and CdTe thin film photovoltaic (PV) devices technologies [1–3] and the high achieved record of conversion efficiency 20.4 % for CdTe based solar cell, they have limitations. Tellurium, indium and gallium are high cost and non abundant on Earth's crust, furthermore cadmium is toxic element [4–8].

Owing to its large absorption coefficient ($\alpha > 10^4$ cm⁻¹) [9–12] and promising photovoltaic properties [13], widespread attention has been focused on Cu–Zn–Sn–S (CZTS) and Cu–Sn–S (CTS) materials to be used in new generation of thin films solar cells. As it contains non-toxic, low cost and abundant elements, it has high potential for mass production as absorber layers [14, 15]. Furthermore, recent computations confirmed by experiments suggest that Cu₂SnS₃ is the most promising compound in the Cu–Sn–S system because of its wide stability range and lack of Fermi level pinning [16].

CTS and CZTS(Se) based thin film solar cells have been synthesised with conversion efficiency 2.7 % [17], 2.84 % [18], 11.1 % [19], however, the most efficient thin film solar cells currently using the CZTSSe as absorber layers gave laboratory efficiency of 12.6 % [20].

Thin CTS films have been made using several techniques, spin coating [21–24], pulsed laser deposition from Cu₂SnS₃ multicomponent targets [25]; doctor blade method [26] nano ink [27]; spray pyrolysis [28, 30]; direct liquid coating [31, 32]; sulfurizing Cu/Sn stacked precursors deposited on glass substrates by electron beam

✉ H. Dahman
h_dahman_2000@yahoo.com

¹ Laboratory of Physics of Materials and Nanomaterials Applied at Environment (LaPhyMNE), Faculty of Sciences, Gabes University, Gabès, Tunisia

² Department of Physics, College of Sciences, Al Imam Mohammad Ibn Saud Islamic University (IMSIU), Riyadh 11623, Saudi Arabia

evaporation [33], sulfurizing, (Cu, Sn)S structured precursors prepared by successive ionic layer absorption and reaction (SILAR) [34, 35]; annealing in sulphur atmosphere electrodeposited metals [18, 36]; heat treatment of electrodeposited SnS–Cu layers [37], sulfurization of DC magnetron sputtered Sn–Cu stacks [38–41], direct evaporation of a synthesized Cu_2SnS_3 powder [42], three steps method based on sulfurization of evaporated copper on sprayed SnS₂ film [43], sulfurization of a stack of vacuum-evaporated Cu and Sn films [44–46] route earlier used by Rezig and Dahman to prepare thin films of iron pyrite [47, 48].

In this study, pure cubic structure Cu_2SnS_3 films were grown by simple one-step spin coating technique from a single precursor's solution of Cu–Sn–thiourea complex. The samples were synthesized at constant temperature with various drying times and have been characterized by several techniques: X-ray diffraction (XRD), atomic force microscopy (AFM), scanning electron microscopy (SEM), optical and four probe analysis.

2 Experimental

Thin CTS films were grown using spin coating route on glass substrates. The substrates were first cleaned by successive ultrasonic bath during 15 min, of acetone, deionised water and ethanol respectively and dried with jet dried-air. All the reagents and solvents were used without further purification. Copper acetate monohydrate $\text{C}_4\text{H}_6\text{CuO}_4\cdot\text{H}_2\text{O}$ (1 mmol), tin chloride dehydrate $\text{SnCl}_2\cdot 2\text{H}_2\text{O}$ (0.5 mmol) and thiourea H_2NCSNH_2 (1.5 mmol), were used as precursors for copper, tin and sulphur respectively. Further experimental details were given in our previous work [21]. The precursors were dissolved into 20 ml methanol and the mixture was then stirred at 60 °C during 2 h to yield a clear and homogenous solution. The resultant solution was spin-coated using the spin coater Model P6700. The films were dried in air on hot plate at constant temperature of 300 °C for several times 2 (S1), 5 (S2), 7 (S3) and 10 min (S4). To obtain the final film, the spin coating and drying steps were repeated five times.

The phase present in the samples materials was identified by using Bruker D5005 diffractometer with $\text{Cu K}\alpha_1$ radiation ($\lambda = 1.5418 \text{ \AA}$) operating at 40 kV, 40 mA. The microstructure of the films was carried out using Veeco DI CP-II Atomic Force Microscope and Field Emission Scanning Electron Microscope (FEI SEM, NNL 200, Japan). The optical properties were investigated, in the range 400–2000 nm, by using Shimadzu 3101PC UV–visible–infrared spectrophotometer. Four probe Lucas Labs-Pro4 was used to measure the sheet electrical resistance of the films. DekTak profilometer was used to measure film thickness and found to be 500–600 nm.

3 Results and discussion

3.1 Structural results

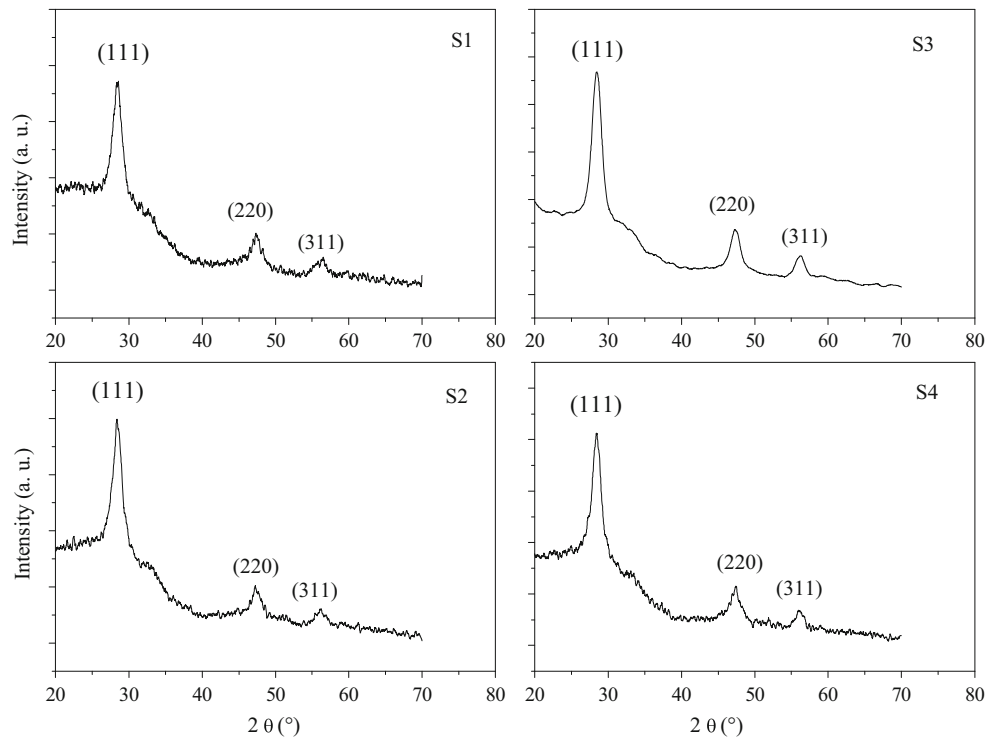
Figure 1 shows the X-ray diffraction patterns of the synthesized thin films on glass substrates for various drying times at 300 °C. For all recorded patterns, three pronounced diffraction peaks were observed at $2\theta = 28.417^\circ$, 47.312° and 56.115° which can be attributed respectively to (111), (220) and (311) planes of Cu_2SnS_3 cubic structure according to JCPDS File no. 89–2877. No other XRD lines are detected signifying that synthesized materials are devoid of any impurity. The observed peaks indicate the polycrystalline nature of the materials. The presence of strong principal diffraction line corresponding to (111) plane indicates that the obtained films may have a preferential orientation.

One can note that our synthesis protocol seems to be the simplest one to obtain pure CTS thin films. Indeed, Kharaman et al. [22], Yaşart et al. [23] used many steps including sulfurization one at 550 °C, while Huan et al. [24] baked the synthesized films, at 80 °C for 5 min, then at 425 °C for 2 min and finally at 600 °C in sulfur atmosphere for 20 min.

Varieties of material structures have been reported in literature: cubic [6, 34, 48–50], tetragonal [22, 23, 32–35, 38, 39, 50, 51–53], monoclinic [36, 37, 54], triclinic [24, 29, 55, 56] and hexagonal phases [30, 57]. The CTS polymorph is strongly affected by the grown temperature, however the influence of other parameters such as stoichiometry of the elements is not excluded. Chalapathi et al. observed on sprayed films that the samples exhibit polymorphism with tetragonal and monoclinic CTS phases. While the as-deposited and annealed films at 400 and 450 °C contain tetragonal as well as monoclinic phases, the films annealed at 500 °C are found to be mostly monoclinic CTS [30]. CTS films deposited at 150 °C using PLD technique clearly indicates tetragonal structure whereas at 250 °C the diffraction peaks consistently match of CTS cubic phase with other phases such as Cu_4SnS_3 and SnS [24]. Films grown by sulfurization of DC magnetron sputtered Sn–Cu metallic precursors in a S2 atmosphere exhibited tetragonal, cubic and orthorhombic structures when sulfurized at 350, 400 and 520 °C respectively [37].

In a recent study, Baranowski et al. observed the zinc blende derived cubic structure of Cu_2SnS_3 as a single phase over a Cu-rich composition range. This wide phase suggests that the material may contain a large Cu on Sn antisite defect concentration or that allowing with a neighboring Cu-rich phase may be occurring [41]. Nevertheless, Aihara et al. [46] has reported, on materials grown by the sulfurization of evaporated Cu–Sn precursors, that

Fig. 1 XRD patterns of grown thin films at 300 °C at various drying times



cubic CTS phase was obtained in the case of Sn-rich samples, while lines detected in Cu-rich materials could be attributed to monoclinic polymorph. In our recent work [58], Cu_2SnS_3 nanoparticles synthesized by solvothermal route exhibited pure cubic phase. The same structure was also observed on nanoparticles elaborated by microwave irradiation [59].

The analysis of reported works revealed controversy results concerning the effect of both grown temperature and elements stoichiometry on material structure. However more investigations will be needed to understand the origin of the CTS materials polymorphs and their obvious influence on their optical and electrical properties.

The average sizes (D) of the samples crystallites can be estimated according to the Debye–Scherrer formula:

$$D = \frac{0.9\lambda}{\beta \cos\theta} \quad (1)$$

where λ is the used X-ray radiation wavelength, β the full width half maximum (FWHM) and θ is the peak Bragg angle.

After a correction for the instrumental broadening, an average value of the crystallites is found to be 6.9–8.2 nm. The calculated interdistance planes (d), the lattice parameter (a) and the average grain size (D) values are summarized in Table 1.

The lattice parameters values are in good agreement with those reported by Fernandes et al. [38] on sample with cubic phase sulfurized at 400 °C: $a_{111} = 5.434 \text{ \AA}$, $d_{111} = 3.14 \text{ \AA}$.

Table 1 Interdistance planes, lattice parameter and crystallite size values for grown films

Sample	t (min)	d_{111} (Å)	a_{111} (Å)	D (nm)
S1	2	3.142	5.442	6.9
S2	5	3.138	5.435	6.7
S3	7	3.140	5.438	7.8
S4	10	3.140	5.438	8.2

However the obtained grain sizes are comparable to those reported by Tiwari [32] and lower than those reported by Kahraman [22] and Yaşar [23] on samples synthesized by spin coating route. Table 2 shows reported results on materials synthesized by several techniques.

As can be seen, the highest crystallite sizes were obtained by sulfurization of sputtered metals while samples grown by chemical based route exhibited crystallites sizes less than 40 nm.

3.2 Microstructure analysis

Atomic force microscopy is one of the most effective means for the surface analysis. It is a non-invasive and convenient technique to study the morphological characteristics and surface roughness of semiconductor thin films and to observe microstructure of CTS layers.

Table 2 Structure and crystallite size of CTS material for several techniques

Preparation technique	Film structure	Crystallite size D (nm)	Ref.
Spin coating	Cubic	7.5	Our result
	Tetragonal	17–25	[22, 23]
Spray pyrolysis	Monoclinic–tetragonal	15–40	[30]
	Triclinic	7–30	[29]
SILAR	Tetragonal	20–40	[35]
Direct liquid coating	Tetragonal	6	[32]
Sulfurization of sputtered metals	Tetragonal	83–229	[38]
	Tetragonal	60	[39]
Heat of electrodeposited SnS–Cu layers	Monoclinic	13	[37]

The surface morphology analysis of deposited films on glass substrates by 2D and 3D AFM are shown in Fig. 2. According to these micrographs, it is evident that the surfaces were rough compact without any visible cracks or holes. These characteristics are suitable to avoid shunting problems in solar cells. Furthermore, large grain size is preferred in the aim to reduce recombination at grain boundaries and involve carrier transport within the grain [60]. As can be depicted from micrographs shown in Fig. 2, the root mean square roughness (RMS) increases from 8 to 68 nm with increasing drying time from 2 to 10 min. The Fig. 3a shows (500 × 500) nm² 2D AFM micrograph of S₃ sample exhibiting agglomeration-like morphology. The observed grain size is higher than crystallite size calculated from XRD results using Scherrer equation. The difference between crystallite size and grain size was explained that grains may be formed by several crystallites. This phenomenon was also observed by other

researchers, Elarbi et al. in thermal evaporated Sn₃Sb₂S₆ thin films [61] and Ares et al. [62] in polycrystalline pyrite films. However from top view SEM micrographs of samples surfaces, except for S₁, were covered partially by homogeneous spherical shape microcrystallites. Figure 3c, d show typical SEM photos for S₁ and S₃ samples. The microcrystallites diameters are ranging between 200 and 600 nm depending on drying time. Similar microcrystallites sizes (200–500 nm) were observed on surface samples grown using spray pyrolysis [63]. The observation was related to the possible vaporization of small drops during film growth. Droplets with dimensions ranging from hundreds of nanometers up to one micron have been observed on surfaces films synthesized by pulsed laser deposition route [25]. In our case, the drying time seems to affect the surface quality of the deposited film and may be the cause of the presence of such forms. At increasing drying time more particles on the surface may agglomerate to form

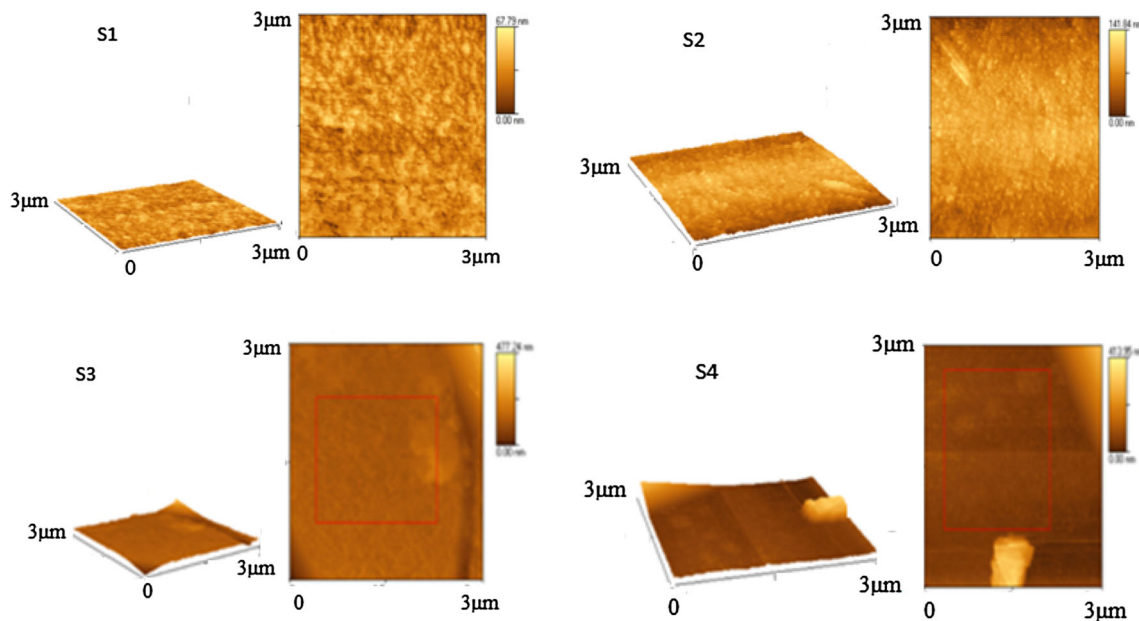
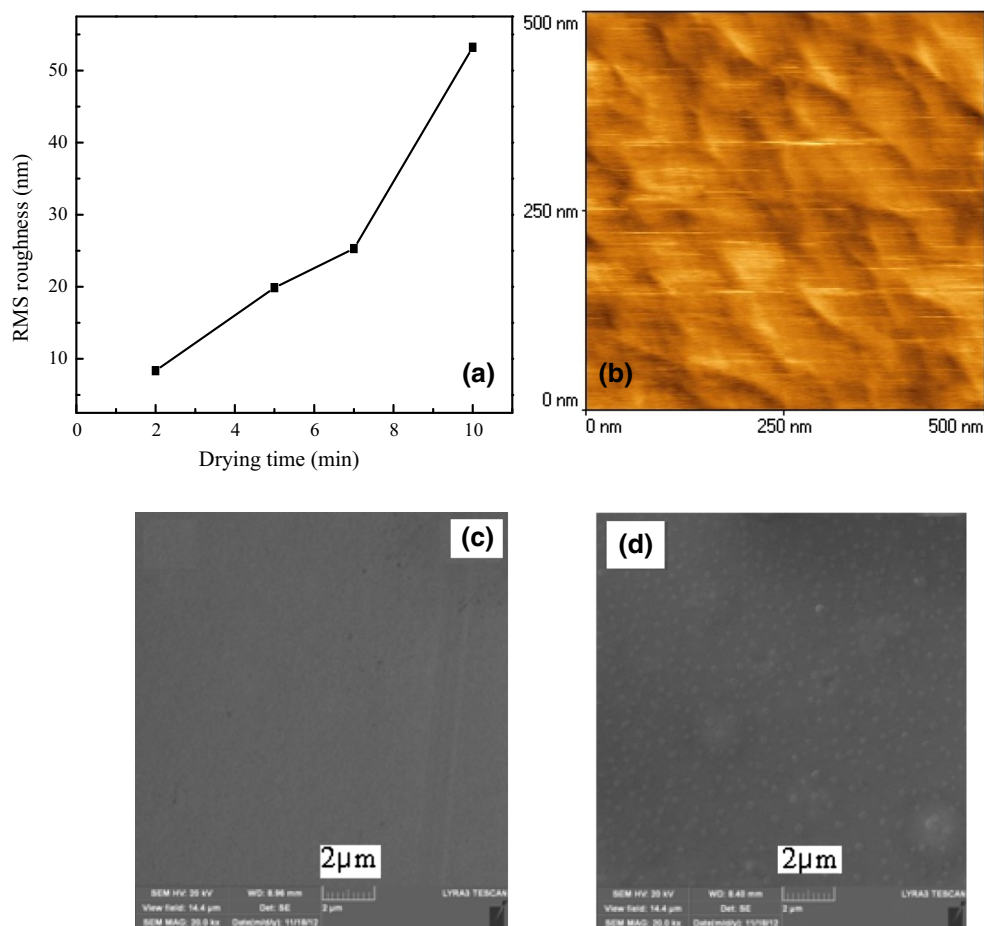


Fig. 2 2D and 3D AFM micrographs for S₁, S₂, S₃ and S₄ samples, scale (3 × 3) μm²

Fig. 3 **a** RMS roughness versus drying time, **b** 2D AFM (500×500) nm² for S₃ sample, *top view* SEM micrographs of **c** S₁ and **d** S₃ samples (scale 2 μm)



bigger grains. Other parameters such as drying temperature, solution viscosity and spinning speed may affect the surface film morphology.

3.3 Optical analysis

Figure 4 shows results of transmittance, absorbance, and absorption coefficient measurements of the synthesised films in the wavelength range 400–2000 nm. From Fig. 4a, the transmittance of S₃ and S₄ is very low for $\lambda < 650$ nm and increases for higher wavelengths, however for S₁ and S₂ samples, the transmittance is very low in the whole visible range and increases for $\lambda > 860$ nm.

The UV–Vis–NIR absorbance measurements shown in Fig. 4b indicate that the material present a broad absorption in a wide wavelength range.

The absorption coefficient $\alpha(h\nu)$ was calculated using the following equation [64]:

$$\alpha = \frac{1}{d} \ln \left[\frac{1 - R}{T} \right] \quad (2)$$

where d is the sample thickness, R and T are respectively the reflectance and the transmittance of the film.

The variation of the absorption coefficient α with the incident energy is shown in Fig. 4c. These curves exhibit large absorption coefficient $\alpha > 310^4$ cm⁻¹ in UV–Vis range for all synthesised films, while $\alpha > 610^4$ cm⁻¹ for S₁ and S₂ samples. From Fig. 4c, one can also notate for S₁, that $\alpha > 10^5$ cm⁻¹ for wavelengths less than 600 nm indicating the high absorbing quality of the film.

The band gap energy E_g is related to absorption coefficient within Tauc formula:

$$\alpha h\nu = A(h\nu - E_g)^n \quad (3)$$

where α is the absorption coefficient, A , $h\nu$ and E_g are respectively constant, incident photon energy and the optical gap, $n = 1/2$ for a direct allowed transition and $n = 2$ for an indirect allowed transition. For direct transition, the band-gap energy of the material is determined by extrapolating the linear region of the plot of $(\alpha h\nu)^2$ versus photon energy ($h\nu$) as shown in Fig. 5a. The point of the extrapolation of the linear part that meets the abscissa will give the value of the material band gap energy. The Fig. 5b presents the variation of E_g versus drying time and outlines a globally increasing in gap energy by increasing drying time. The obtained values 1.19–1.65 eV, are suitable for

Fig. 4 **a** Transmittance, **b** absorbance, **c** absorption coefficient versus $h\nu$ (eV) of grown samples

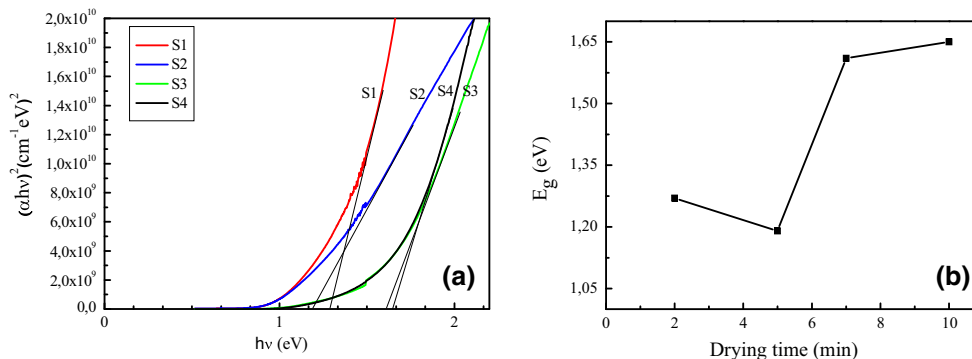
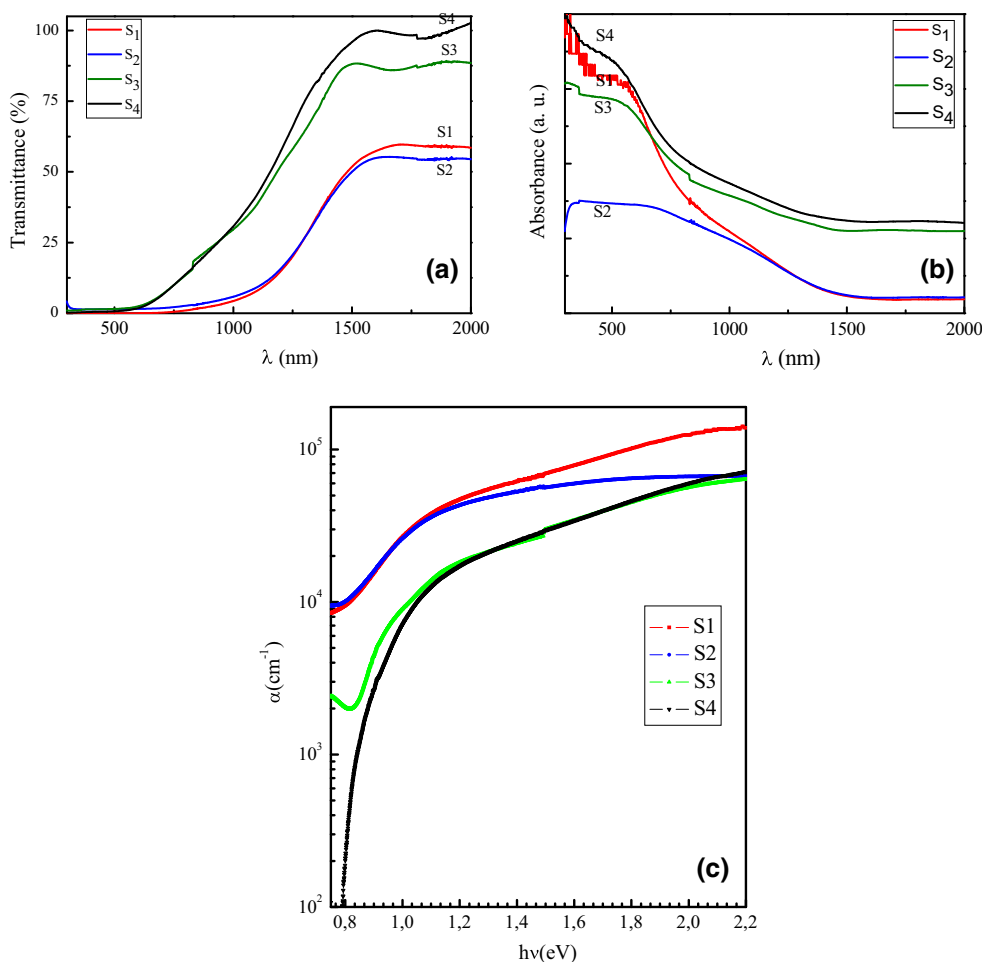


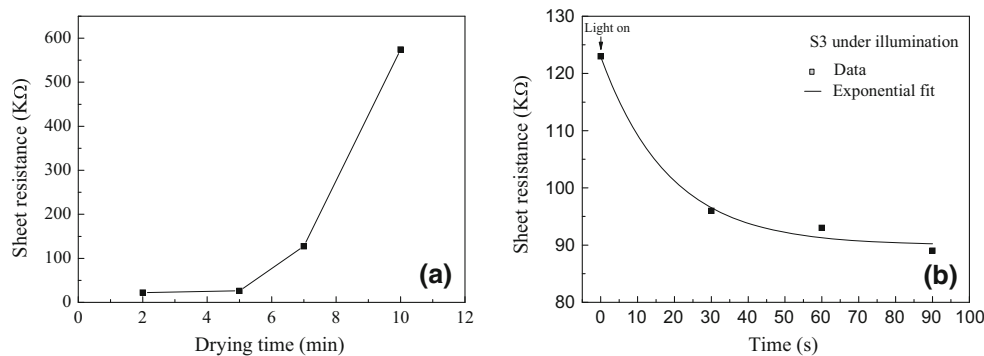
Fig. 5 **a** Tauc plots, **b** gap energy versus drying time

photovoltaic solar conversion and in good agreement with reported values obtained by spray pyrolysis 0.93–1.65 eV depending on grown temperature [30]. However, samples grown by RF magnetron sputtering at temperatures of 350–425 °C in hydrogen sulfide and nitrogen atmosphere, showed band gap in the range 1.77–2.19 eV [65]. Whereas smaller values were reported for thin films synthesised by other techniques [12, 17, 35, 37].

3.4 Sheet resistance measurement

The film sheet resistance R_γ variation versus drying time is shown in Fig. 6a. A clearly increasing in R_γ can be observed. The sheet resistance increases from 22 to 575 k Ω when drying time increases from 2 to 10 min. Spectral shifts of the energy gap as a function of the growth parameters have been reported by several groups, the results

Fig. 6 **a** Sheet resistance versus drying time, **b** S_3 sheet resistance under illumination versus time



being rather confusing. In our case, we have seen an increase of optical energy gap and the sheet resistance with the drying time. This effect was observed by Hamburg and Granquist [66] and attributed to the combined effects of a Burstein–Moss shift and impurity scattering. The increase of the optical band gap can be attributed also to the increase of the grain boundaries and crystal defects.

The Fig. 6b exhibits the sample sheet resistance evolution versus time for sample S_3 under polychromatic light excitation of about 300 mW/cm^2 . The observed light sensibility of the film leads to think that material is a promising candidate for photovoltaic applications. Photo-current activity was observed on structures based on Cu_2SnS_3 materials grown, by spin coating technique [23], sulfurization of electron beam evaporated Cu–Sn alloy [17] and by sulfurization of electrodeposited SnS–Cu layers [37].

4 Conclusion

Thin films of the ternary Cu_2SnS_3 material was successfully synthesised by simple one-step spin coating technique at constant drying temperature of $300 \text{ }^\circ\text{C}$ during several times. The X-ray diffraction results show that the obtained layers was composed by a pure single cubic phase Cu_2SnS_3 with (111) preferential orientation without any secondary phases. The calculated crystallite sizes using Debye–Scherer formula were found about 7.5 nm. SEM and AFM analysis revealed good surface morphology without any cracks or holes. The room temperature sheet resistance increases significantly from 22 to 575 $\text{K}\Omega$ with increasing drying time from 2 to 10 min and shows a visible light sensibility. The deposited films exhibited high optical absorption coefficient $\alpha > 310^4 \text{ cm}^{-1}$ for $\lambda < 1200 \text{ nm}$ and $\alpha > 10^5 \text{ cm}^{-1}$ in the range 400–690 nm for sample dried for 2 min. We found that by increasing the drying time, the direct optical band gap increased from 1.19 to 1.65 eV which is optimum for photovoltaic solar conversion. The found results make the material as good candidate as absorber layer in low cost, friendly environment and flexible solar cells.

Acknowledgments The authors would like to thank Dr. A. Alyamani for morphological analysis.

References

- M.A. Green, K. Emery, Y. Hishikawa, W. Warta, *Prog. Photovolt. Res. Appl.* **17**, 85–94 (2009)
- M.A. Green, K. Emery, Y. Hishikawa, W. Warta, *Prog. Photovolt. Res. Appl.* **18**, 346–352 (2010)
- D. Butler, *Nature* **454**, 558–559 (2008)
- J.J. Scragg, P.J. Dale, L.M. Peter, G. Zoppi, I. Forbes, *Phys. Status Solidi B* **245**, 1772–1778 (2008)
- H. Deligianni, S. Ahmed, L.T. Romankiw, *Interface* **20**, 47–53 (2011)
- N.S. Lewis, D.G. Nocera, *Proc. Natl. Acad. Sci. USA* **103**, 15729–15735 (2006)
- C. Wadia, A.P. Alivisatos, D.M. Kammen, *Environ. Sci. Technol.* **43**, 2072–2077 (2009)
- B.A. Anderson, *Prog. Photovolt. Res. Appl.* **8**, 61–76 (2000)
- K. Jimbo, R. Kimura, T. Kamimura, S. Yamada, W.S. Maw, H. Araki, K. Oishi, H. Katagiri, *Thin Solid Films* **515**, 5997–5999 (2007)
- H. Katagiri, *Thin Solid Films* **480**, 426–432 (2005)
- H. Katagiri, K. Saitoh, T. Washio, H. Shinohara, T. Kurumadani, S. Miyajima, *Sol. Energy Mater. Sol. Cells* **65**, 141–148 (2001)
- M. Bouaziz, M. Amlouk, S. Belgacem, *Thin. Sol. Films* **517**, 2527–2530 (2009)
- S.W. Shin, J.H. Han, Y.C. Park, G.L. Agawane, C.H. Jeong, J.H. Yun, A.V. Moholkar, J.Y. Lee, J.H. Kim, *J. Mater. Chem.* **22**, 21727–21732 (2012)
- R.A. Wibowo, W.S. Kim, E.S. Lee, B. Munir, K.H. Kim, *J. Phys. Chem. Solids* **68**, 1908–1913 (2007)
- L.J. Chen, Y.J. Chuang, *J. Cryst. Growth* **376**, 11–16 (2013)
- P. Zawadzki, L.L. Baranowski, H. Peng, E.S. Toberer, D.S. Ginley, W. Tumas, A. Zakutayev, S. Lany, *Appl. Phys. Lett.* **103**, 253902 (2013)
- N. Aihara, A. Kanai, K. Kimura, M. Yamada, K. Toyonaga, H. Araki, A. Takeuchi, H. Katagiri, *Jpn. J. Appl. Phys.* **53**, 05FW13 (2014)
- J. Koike, K. Chino, N. Aihara, H.A. Nakamura, K. Jimbo, H. Katagiri, *Jpn. J. Appl. Phys.* **51**, 10NC34 (2012)
- T.K. Todorov, J. Tang, S. Bag, O. Gunawan, T. Gokmen, Y. Zhu, D.B. Mitzi, *Adv. Energy. Mater.* **3**, 34–38 (2013)
- W. Wang, M.T. Winkler, O. Gunawan, T. Gokmen, T.K. Todorov, Y. Zhu, D.B. Mitzi, *Adv. Energy. Mater.* **4**, 1301465 (2014)
- H. Dahman, S. Rabaoui, A. Alyamani, L. El Mir, *Vacuum* **101**, 208–211 (2014)

22. S. Kahraman, S. Çetinkaya, S. Yaşar, İ. Bilican, *Phil. Mag.* **94**, 3149–3161 (2014)
23. S. Yaşar, S. Kahraman, S. Çetinkaya, İ. Bilican, *J. Alloy. Compd.* **618**, 217–221 (2015)
24. J. Han, Y. Zhou, Y. Tian, Z. Huang, X. Wang, J. Zhong, Z. Xia, B. Yang, H. Song, J. Tang, *Front. Optoelectron.* **7**, 37–45 (2014)
25. R.B. Ettliger, A. Cazzaniga, S. Canulescu, N. Pryds, J. Schou, *Appl. Surf. Sci.* **336**, 385–390 (2015)
26. Q. Chen, X. Dou, Y. Ni, S. Cheng, S. Zhuang, *J. Colloid Interface Sci.* **376**, 327–330 (2012)
27. S.A. Vanalakar, G.L. Agawane, S.W. Shin, H.S. Yang, P.S. Patil, J.Y. Kim, J.H. Kim, *Acta Mater.* **85**, 314–321 (2015)
28. M. Bouaziz, J. Ouerfelli, M. Amlouk, S. Belgacem, *Phys. Status Solidi A* **204**, 3354–3360 (2007)
29. M. Adelifard, M.M.B. Mohagheghi, H. Eshghi, *Phys. Scr.* **85**, 035603–035608 (2012)
30. U. Chalapathi, Y. Jayasree, S. Uthanna, V. Sundara Raja, *Phys. Status Solidi A* **210**, 2384–2390 (2013)
31. D. Tiwari, T.K. Chaudhuri, T. Shripathi, U. Deshpande, *AIP Conf. Proc.* **1447**, p1039 (2012)
32. D. Tiwari, T.K. Chaudhuri, T. Shripathi, U. Deshpande, R. Rawat, *Sol. Energy Mater. Sol. Cells* **113**, 165–170 (2013)
33. K. Chino, J. Koike, S. Eguchi, H. Araki, R. Nakamura, K. Jimbo, H. Katagiri, *Jpn. J. Appl. Phys.* **51**, 10NC35-1–10NC35-4 (2012)
34. H. Guan, H. Shen, C. Gao, X. He, *J. Mater. Sci.: Mater. Electron.* **24**, 1490–1494 (2013)
35. Z. Su, K. Sun, Z. Han, F. Liu, Y. Lai, J. Li, Y. Liu, *J. Mater. Chem.* **22**, 16346–16352 (2012)
36. D.M. Berg, R. Djemour, L. Gutay, S. Siebentritt, P.J. Dale, X. Fontane, V. Izquierdo-Roca, A. Pérez-Rodríguez, *Appl. Phys. Lett.* **100**, 192103–192106 (2012)
37. N.R. Mathews, J. Tamy Benítez, F. Paraguay-Delgado, M. Pal, L. Huerta, *J. Mater. Sci.: Mater. Electron.* **24**, 4060–4067 (2013)
38. P.A. Fernandes, P.M.P. Salome, A.F. da Cunha, *J. Phys. D Appl. Phys.* **43**, 215403–215414 (2010)
39. R. Bodeux, J. Leguay, S. Delbos, *Thin Solid Films* **618**, 222–226 (2014)
40. H. Zhang, M. Xie, S. Zhang, Y. Xiang, *J. Alloys Compd.* **602**, 199–203 (2014)
41. L.L. Baranowski, P. Zawadzki, S. Christensen, D. Nordlund, S. Lany, A.C. Tamboli, L. Gedvilas, D.S. Ginley, W. Tumas, E.S. Toberer, A. Zakutayev, *Chem. Mater.* **26**, 4951–4959 (2014)
42. T.A. Kuku, O.A. Fakolujo, *Sol. Energy Mater.* **16**, 199–204 (1987)
43. A. Amlouk, K. Boubaker, M. Amlouk, *Vacuum* **85**, 60–65 (2010)
44. A.J. Cheng, M. Manno, A. Khare, C. Leighton, S.A. Campell, E.S. Aydil, *J. Vac. Sci. Technol. A* **29**, 051203–051214 (2011)
45. M. Bouaziz, J. Ouerfelli, S.K. Srivastava, J.C. Bernède, M. Amlouk, *Vacuum* **85**, 783–786 (2011)
46. N. Aihara, H. Araki, A. Takeuchi, K. Jimbo, H. Katagiri, *Phys. Status Solidi C* **10**, 1086–1092 (2013)
47. B. Rezig, H. Dahman, M. Kenzari, *J. Renew. Energy* **2**, 125–128 (1992)
48. H. Dahman, M. Khalifa, B. Rezig, M. Brunel, *Thin Solid Films* **280**, 56–60 (1996)
49. G. Moh, *Chem. Erde* **34**, 1–61 (1975)
50. P.A. Fernandes, P.M.P. Salome, A.F. da Cunha, *Phys. Status Solidi.* **7**, 901–904 (2010)
51. X. Liang, Q. Cai, W. Xiang, Z. Chen, J. Zhong, Y. Wang, M. Shao, Z. Li, *J. Mater. Sci. Technol.* **29**, 231–236 (2013)
52. H. Hahn, H. Schulze, *Naturwissenschaften* **52**, 426 (1965)
53. N. Wang, *N. Jahrb. Mineral.* **241**, 424–431 (1974)
54. M. Onoda, X.A. Chen, A. Sato, H. Wada, *Mater. Res. Bull.* **35**, 1563–1570 (2000)
55. X. Chen, X. Wang, C. An, J. Liu, Y. Qian, *J. Cryst. Growth* **256**, 368–376 (2003)
56. D. Avallaneda, M.T.S. Nair, P.K. Nair, *J. Electrochem. Soc.* **187**, D346–D352 (2010)
57. C. Wu, Z. Hu, C. Wang, H. Sheng, J. Yang, Y. Xie, *Appl. Phys. Lett.* **91**, 143104–143106 (2007)
58. S. Rabaoui, H. Dahman, N. Ben Mansour, L. El Mir, *J. Mater. Sci.: Mater. Electron.* **26**, 1119–1124 (2015)
59. W. Wei, S. Honglie, L. Jinze, *Mater. Lett.* **111**, 5–8 (2013)
60. Q.W. Tian, X.F. Xu, L.B. Han, M.H. Tang, R.J. Zou, Z.G. Chen, M.H. Yu, J.M. Yang, J.Q. Hu, *Cryst. Eng. Comm.* **14**, 3847–3850 (2012)
61. A. Larbi, H. Dahman, M. Kanzari, *Vacuum* **110**, 34–39 (2014)
62. J.R. Ares, A. Pascual, I.J. Ferrer, C. Sánchez, *Thin Solid Films* **480**, 477–481 (2005)
63. M. Bouaziz, K. Boubaker, M. Amlouk, S. Belgacem, *J. Phase Equilibria Diffus.* **31**, 498–503 (2010)
64. M. Balkansk, T.S. Moss, *Optical properties of semiconductors* (Elsevier Science & Technology Books, Amsterdam, 1994)
65. P. Zhao, S. Cheng, *Adv. Mater. Sci. Eng.* 726080 (2013)
66. I. Hamburg, C.G. Granquist, *J. Appl. Phys.* **60**, 123 (1986)